Impact of wind conditions on thermal loading of PMSG wind turbine power converters

C J Smith, C J Crabtree*, P C Matthews**

**School of Engineering and Computing Sciences, Durham University, United Kingdom, c.j.smith2@dur.ac.uk, c.j.crabtree@dur.ac.uk, p.c.matthews@dur.ac.uk*

Keywords: Power converter, thermal loading, reliability.

Abstract

Power converter reliability is critical for permanent magnet synchronous generator (PMSG) wind turbines. Converter failures are commonly linked to the power module thermal loading. This paper models the expected converter thermal loading when the turbine is subjected to various synthetic wind speed conditions, including constant and square wave profiles. It was found that the model performed as expected compared to manufacturer's data and the diodes had greater thermal loading than the insulated-gate bipolar transistors (IGBTs). The preliminary results from synthetic square wave wind speed time series (WSTS) suggest that wind events with a period >5s are critical to the device thermal loading.

1 Introduction

To meet EU renewable energy targets for 2020 and beyond, the Levelised Cost of Energy (LCoE) of offshore wind needs to be reduced to below £100/MWh [1]. Operation and maintenance (O&M) accounts for approximately 30% of the LCoE [2]. A key aspect of O&M is the reliability of the turbine sub-systems. By understanding which components' reliability has the greatest impact on downtime and power production, O&M resources can be focused to minimise turbine disruption and reduce offshore wind's LCoE.

A number of studies have explored the reliability of wind turbine sub-systems. [3] examined a large dataset for offshore wind turbines with varying turbine technology to determine the main causes of failure and concluded that the power converter had a typical failure rate of ~0.2 failures/turbine/year (f/t/y), which was much lower than the highest failure rate of >1 f/t/y for the pitch system. However, a more focused study on turbine type [4] found that the failure rate of fully-rated converters (FRC) in permanent magnet synchronous generator (PMSG) turbines was 0.593 f/t/y compared to the 0.106 f/t/y for doubly fed induction generator (DFIG) turbines. Furthermore, [5] examined large datasets of wind turbines and consulted expert knowledge to produce a top 30 list of turbine failure modes and concluded that the power converter was the highest risk component to turbine reliability. The reliability of the converter must therefore be examined with a focus on the FRC in PMSG turbines.

Of the failures outlined in [4], power module failure is the failure mode for nearly all major converter repairs. Traditionally, this power module failure has been linked to power module thermal loading, where the variation of junction temperature in the insulated gate bipolar transistors ($\Delta T_{j,IGBT}$) and diodes ($\Delta T_{j,diode}$) causes fatigue through expansion and contraction of current carrying components. This is analogous to fatigue in mechanical engineering.

This approach has been applied in a number of studies to explore the expected reliability of power converters in wind turbines [6-15]. However these studies often have limitations:

- Neglect the impact of turbine response by using simplified wind turbine models and/or wind speed inputs.
- Limited scope of failure data. Cycles-to-failure is derived from manufacturer or experimental data which consider only fixed magnitude ΔT_j, implying a fixed input current.
- Limited validation approaches. Experimental work is often carried out at constant input conditions.

These limitations mean that the operational profiles and failure data are not representative of how a converter operates in the field. In response these research questions were formed.

1. Are the thermal loading profiles generated in the power modules verifiable for complex input profiles?
2. Which operating conditions cause the greatest thermal loading to the power modules and does this correspond to the greatest damage?
3. Is the use of manufacturing cycles-to-failure data a valid approach for converter lifetime estimation under complex loading conditions such as operation in a wind turbine?

This paper concentrates on providing the benchmark for the 3 questions by modelling the expected thermal loading and finding the wind conditions which theoretically cause the greatest damage to the converter.

The paper is organised as follows. Section 2 outlines the approach for producing the thermal loading profiles, including a drive train model (Section 2.1), power loss model (Section 2.2), thermal model (Section 2.3) and wind inputs (Section 2.4). Section 3 outlines the thermal loading results from simulations and Section 4 concludes the work.

2 Approach

To determine the thermal loading of a wind turbine power converter the following procedure was followed:

1. Model a wind turbine drive train to provide the current throughput of the converter.
2. Model the resultant power losses in the converter due to the current throughput.
3. Model the power module thermal processes in response to the power losses.
4. Simulation of power module thermal response to a variety of wind speed inputs.

This section outlines the details of each step.

2.1 Drive Train Model

To ensure an accurate current throughput is provided the turbine dynamics need to be considered. A drive train model has been constructed previously for this purpose [16]. The following summarises the model's key details.

- Modelled as a direct-drive 2MW wind turbine.
- Mechanical drive train modelled as a 2-mass model.
- 2nd order non-salient PMSG.
- FRC based on SEMIKRON RE stacks.
- Grid-side converter (GSC) modelled as an ideal DC link.
- Maximum power point tracking (MPPT) achieved using *dq0* vector control.
- Active pitch control.

Updates have been made to the turbine control for this paper:

1. The reference pitch angle (β_{ref}) is limited to positive values to avoid an issue in the actuator system integration delaying the pitch actuator.

2. The torque controller is no longer constrained by the rated turbine rotational speed ($\omega_{t,rat}$) but by a higher maximum ($\omega_{t,max}$). This allows the torque controller to deal with sudden increases in wind speed that the pitch controller is too slow to respond to effectively. This provides a similar controller interaction as found in [17].

Figure 1.b, d shows an improved pitch control response. This updated control requires a higher converter maximum current throughput ($I_{out,max}$) compared to in [16] (Figure 1.c, e). Therefore the MSC was replaced with two parallel SKSB2100GD69/11-MAPB stacks, providing an $I_{out,max}$ of 1000 A_{rms} per stack [18]. This corresponds to a total I_q of 2828 A, which was reduced to 2800 A to allow for noise and controller overshoot This dictates a $\omega_{t,max}$ of 2.43 rad/s.

The new stacks meant the half-bridge modules used were changed to SKiiP 2013GB172-4DWV3 modules [19]. This made little difference to the drive train parameters except the collector-emitter resistance (R_{on}) was reduced to 0.925 mΩ.

To summarise, a 2MW PMSG wind turbine with a FRC model was used from a previous work [16] with improvements to the turbine control and MSC data used.

2.2 Converter Power Loss Model

To convert the current throughput into power module T_j profiles the power module component power losses much be calculated. This section outlines the power loss model used.

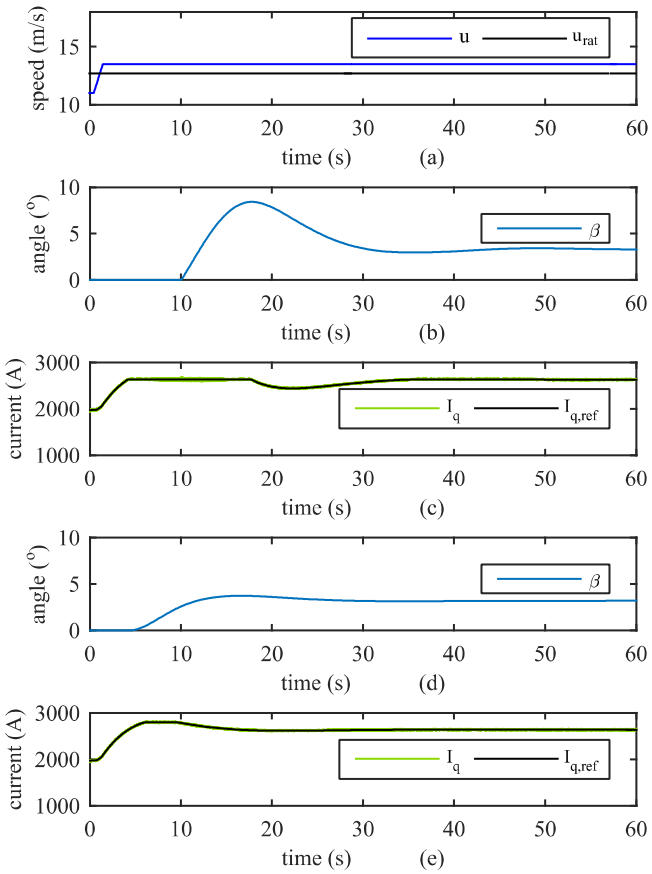

Figure 1: Turbine control update. (b) and (c) are the pitch and I_q response in [16] to a given wind speed input (a). (d) and (e) are the updated pitch and I_q response.

The electrical loss models used in the literature consider losses in IGBTs and diodes. This includes the conduction losses of IGBTs and diodes, the switching losses of the IGBT and the reverse recovery (RR) losses of the diodes [7-10, 20].

The power loss model used is based on the models in [20, 21]. The power losses were calculated as follows:

1. The current throughput of each device is simulated.
2. The IGBT and diode conduction losses are calculated.
3. The IGBT switching losses and diode RR losses are calculated.
4. The conduction and switching losses are summed for each device and fed to the thermal model.

Conduction Losses

The conduction losses are related to the power dissipated from the devices' internal resistance. This is calculated by determining the voltage and current of the device (1, 2).

$$P_{C,IGBT} = V_{ce}\, I_c \quad (1)$$

$$P_{C,diode} = V_f\, I_f \quad (2)$$

Where $P_{C,IGBT}$ and $P_{C,diode}$ are the IGBT and diode conduction losses respectively, V_{ce} is the IGBT collector-emitter voltage, V_f is the diode forward voltage, I_c is the IGBT collector current, and I_f is the diode forward current.

I_c and I_f are the input currents. V_{ce} and V_f are functions of I_c and I_f respectively, and the device T_j. The functions are given in the manufacturer's data sheet [19] for a T_j of 25°C and 125°C. Look-up tables (LUT) have been produced to determine the V_c, and V_f for each time step for these reference T_j. The T_j from the previous time step is used to provide the actual V by linearly interpolating between the reference Vs.

Switching/RR Losses

Switching and RR losses occur when there is a change in direction of voltage and current as these changes are not instantaneous. This occurs in a period of hundreds of nanoseconds [20] so the model fidelity has to be considered.

Simulating over nanoseconds is impractical for times longer than a few seconds. Energy loss information given in manufacturer's datasheets is also not detailed enough for accurate temporal loss simulation. For example, the IGBT energy loss is a total energy loss for both on and off switching events (E_{on+off}) [19]. Splitting this energy equally would not be valid as revealed in other datasheets [22]. This limited information means a simplified approach has to be taken.

It has therefore been assumed that the energy loss is given by the conditions at the first low-high (L-H) switching instance. The energy is modulated over the switching cycle (between L-H and the next L-H) to provide a constant switching power loss. This was deemed acceptable as the device thermal time constants will dominate the thermal profile.

The switching/RR losses are calculated as follows:

1. Determine when the device input changes from L-H.
2. Determine the time period between L-H switching events (T_p). If this time period was found to be greater than a threshold ($T_{p,max}$) the device was deemed to be switched off for a long time and the T_p set to $1/f_{sw,ref,}$ where $f_{sw,ref}$ is the maximum switching frequency of the converter.
3. Determine the energy losses at L-H switching events. The switching/RR energy loss is given as a function of input current at two reference DC voltages (V_{DC}) [19]. Therefore a LUT was constructed for both reference V_{DC}'s and the input current used to determine the corresponding energy loss. The actual V_{DC} is then used to linearly interpolate between these two reference values. For the IGBT this energy loss is the E_{on+off}, whilst the diode energy loss is twice the RR energy loss (E_{rr}).
4. The equivalent modulated power losses over the switching cycle are calculated using (3, 4).

$$P_{sw}(t{:}T_{s,th}{:}\,(t + T_{p,sw}(t))) = \frac{E_{on+off}(t)}{T_{p,sw}(t)} \quad (3)$$

$$P_{rr}(t{:}T_{s,th}{:}(t + T_{p,rr}(t))) = \frac{E_{rr}(t)}{T_{p,rr}(t)} \quad (4)$$

Where P_{sw} is the IGBT switching power loss, P_{rr} is the diode RR power loss, t is the time step, $T_{s,th}$ is the thermal sampling time ($5x10^{-5}$ s), $T_{p,sw}$ is the IGBT switching time period and $T_{p,rr}$ is the diode RR time period.

5. The switching/RR losses are also T_j dependent, with the relationship determined as in (5, 6) [21].

$$P_{sw,T_j}(t) = \left(1 + TC_{Esw}\left(T_{j,IGBT}(t) - T_{ref}\right)\right) P_{sw}(t) \quad (5)$$

$$P_{rr,T_j}(t) = \left(1 + TC_{Err}\left(T_{j,diode}(t) - T_{ref}\right)\right) P_{rr}(t) \quad (6)$$

Where $P_{sw,Tj}$, $P_{rr,Tj}$ are the T_j corrected P_{sw} and P_{rr} respectively, TC_{Esw} TC_{Err} are the switching loss and RR temperature coefficients respectively, and T_{ref} is the reference temperature of the energy loss LUTs.

With the conduction and switching/RR power losses calculated the total power loss can be calculated.

2.3 Thermal Loss Model

Converter thermal modelling is carried out in three ways:

- Thermal equivalent circuits [7-9, 11-14].
- Thermal diffusion equations [10].
- Finite Element Analysis (FEA) [6].

The choice of thermal model is based on data availability and computational efficiency. The thermal equivalent circuits are used when Foster network resistor-capacitor (RC) manufacturing data is available. Modifications are made to improve the network accuracy, which often involves converting to a Cauer network. If this data is not available or detailed device analysis is required, thermal diffusion equations or FEA is used. However these methods are computationally expensive. As the RC network data was available a thermal equivalent circuit was used.

The data given in [19] is for a Foster RC network. This network gives a numerical approximation of the thermal network which means that the calculated temperatures, except T_j and the ambient temperature (T_a), have no physical meaning. To provide a more accurate half-bridge temperature profile the Foster thermal resistance ($R_{th,f}$) and time constant (τ) parameters were converted into RC parameters (7) [23], and then converted into Cauer RC parameters using the algorithm available at [24]. This conversion was carried out independently for each IGBT, diode and heat sink. Figure 2 gives the half-bridge Cauer RC network.

$$C_{th,f} = \frac{\tau}{R_{th,f}} \quad (7)$$

Where $C_{th,f}$ is the Foster thermal capacitance.

Wind Speed Inputs

Wind speed and converter current throughput are decoupled by the turbine inertia and control [16]. As such, determining which characteristics of a wind speed time series (WSTS) have the largest impact on thermal loading is challenging.

To address this, experiments have been constructed which use synthetic WSTS to isolate potential wind speed characteristics and determine their impact on thermal loading. Square waves have been used to represent sudden changes in wind speed. Figure 3 shows an example synthetic WSTS. The constant wind speed at the start is for initialisation (Section 2.5).

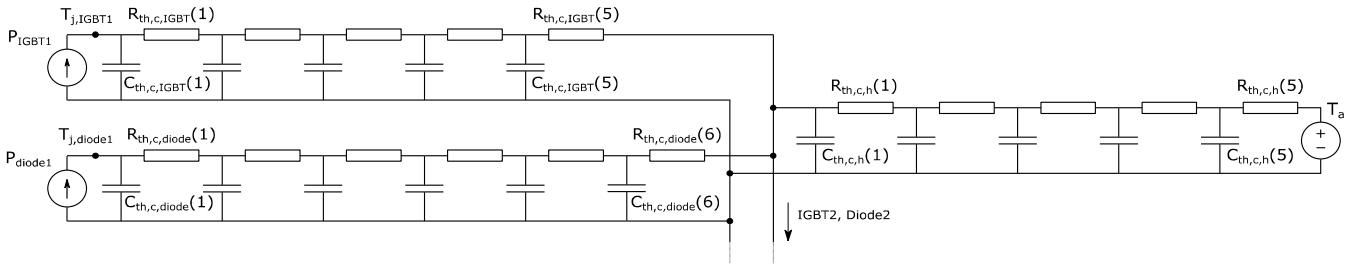

Figure 2: Half bridge Cauer RC network (only one IGBT and diode represented here). P_{IGBT1} is the IGBT power loss, P_{diode1} is the diode power loss, $R_{th,c}$ is the Cauer thermal resistance, $C_{th,c}$ is the Cauer thermal capacitance, and $_h$ is the heat sink.

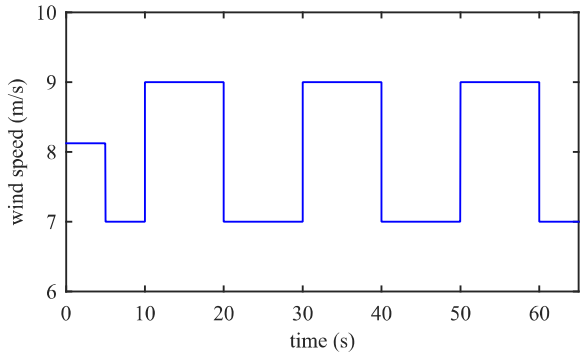

Figure 3: 7-9 m/s, 20s period square wave.

2.4 Overall system

Figure 4 summarises the whole system model.

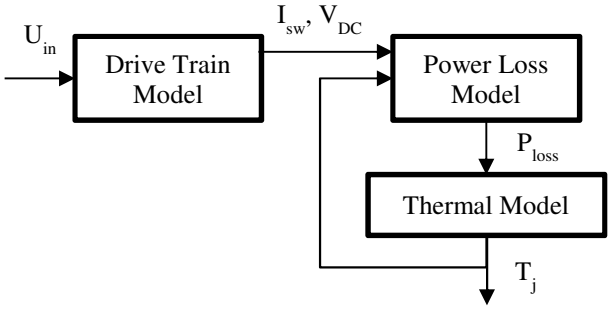

Figure 4: Turbine-converter thermal loading model.

The power losses (P_{loss}) are dependent on T_j and therefore the power loss and thermal sub-systems must be run concurrently. Technically the current throughput of the devices is also related to the power losses and T_j, but it was assumed that this effect would be negligible [20].

Due to the power-thermal inter-dependency the initialisation of C_{th} temperatures was solved iteratively. The steady-state temperatures are related to the R_{th} only [21], with the temperatures analogous of a voltage drop (temperature) due to a current throughput (power). The steps are as follows:

1. Set initial temperatures for each C_{th} (typically to T_a).
2. Take first 0.5s of input current for each device.
3. Calculate power loss over 0.5s given device T_j.
4. Calculate steady state temperatures using R_{th} only.
5. Update device temperatures.
6. Compare previous and new device temperatures. If the variation is less than 0.001°C then the temperatures are deemed correct. Otherwise repeat steps 2-6.

This initialisation is subject to variations in the input current and therefore all tests are carried out with a 5s constant wind speed at the start (Figure 3). For the square wave tests this constant wind speed represents the average power wind speed, which is slightly higher than the average wind speed due to the cubic relationship between wind speed and power.

To summarise, a computer model of a wind turbine drive train and power converter thermal network has been constructed. This allows for any wind speed profile to be entered and the corresponding power module thermal profiles be produced.

3 Results and Discussion

This section outlines the analysis performed on T_j profiles produced in response to constant and square wave WSTS.

3.1 Constant Wind Speeds

Figure 5 shows the thermal response to constant WSTS for IGBT1 and Diode1 with a T_a of 25°C. As expected, the mean T_j increases non-linearly as wind speed increases due to the cubic relationship between wind speed and power. The ΔT_j also increases with increased wind speed due to the higher power loss per cycle, and the ΔT_j frequency increases due to the higher generator rotational speed. Interestingly the diode T_j and ΔT_j (5.a) are consistently higher than the IGBT (5.b). This is due to the higher power losses experienced by the diodes. This was also found for the MSC devices in [11].

The results in Figure 5 were compared to those in [11]. It was found that the T_j and ΔT_j for 12 m/s were similar for both IGBT and diode. However, this similar T_j is misleading as the T_a was 25°C higher in [11]. This suggests that the MSC in this work is more susceptible to T_j rises due to the higher R_{th} values in the devices and heatsink. This is supported by the T_j change from 12 m/s to 8.5 m/s being much lower in [11] than in Figure 5. It also highlights the need to consider T_a.

Figure 6 zooms in on one power loss and T_j cycle. The T_j profile is comparable with the expected response found in Figure 5.2.13 in the manufacturer's handbook [21].

In summary, the devices' T_j response to various constant wind speeds performed as expected, and the diode had a more aggressive thermal response. The individual T_j cycles were consistent with manufacturer's data. This MSC was deemed to be more susceptible to T_j variation than the one in [11] and this difference highlighted the need for an accurate T_a value.

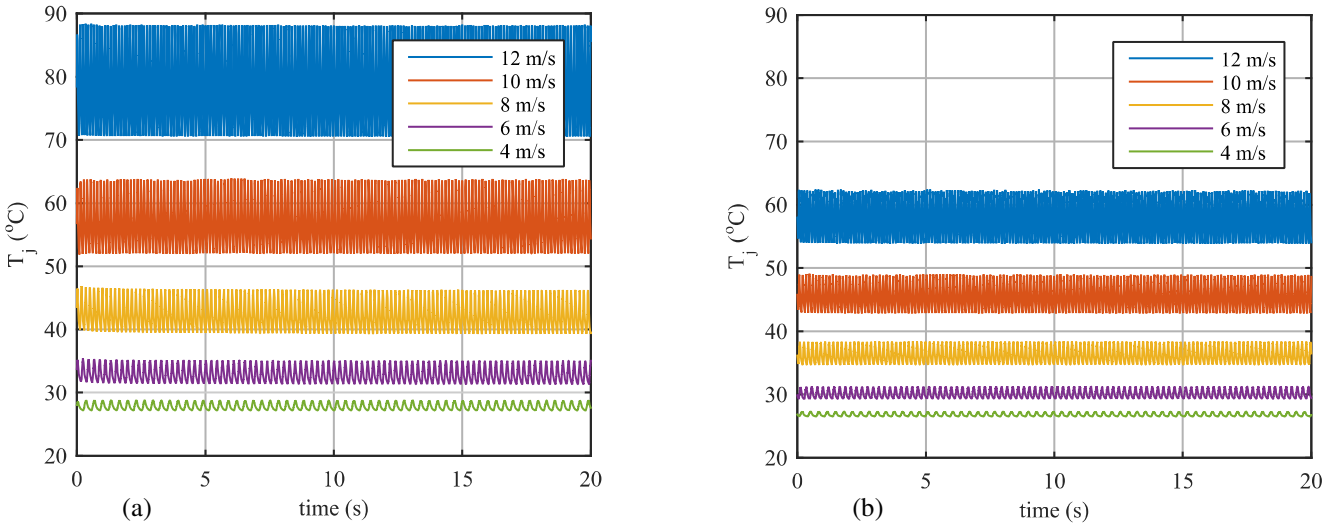

Figure 5: T_j response to constant wind speeds in the MPPT region for (a) Diode1 and (b) IGBT1.

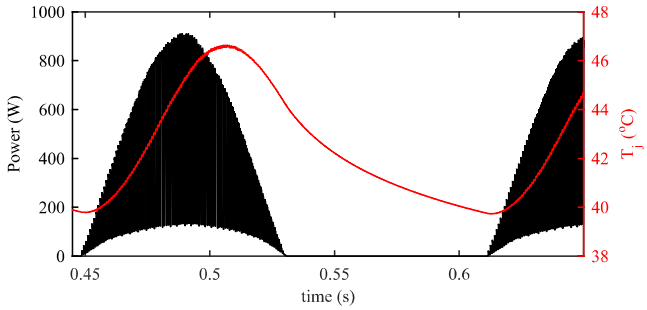

Figure 6: One power loss and T_j cycle for Diode1 at 8m/s.

3.2 Response to Varying Wind Speed input

The T_j response of IGBT1 to a range of square wave WSTS is detailed. For comparison the mean, maximum and minimum T_j ($T_{j,mean}$, $T_{j,max}$, $T_{j,min}$) have been plotted for wave amplitudes of 1 and 2 m/s for varying time periods and mean wind speeds (Figure 7). There are 4 main conclusions from these results:

1. The constant wind speed generally has a lower T_j than the square waves. This is due to the average power being higher than the mean wind speed (U_m) power. Therefore the average wind power must be considered.
2. $T_{j,mean}$ is constant for the square waves for a given U_m.
3. At low time periods (0.5-5s) the temperature range (ΔT) is similar to the constant case (Figure 7). This would suggest that wind speed variations in this period could be neglected for life time estimation, though this assumption needs experimental validation.
4. Between a 5-10s period ΔT becomes significant (Figure 7), particularly for a wave amplitude of 2 m/s (Figure 7.b). This was more pronounced for Diode1. Therefore variations in wind speed over this period cannot be neglected when determining device thermal loading.

4 Conclusions

The wind turbine power converter is reliability critical for FRC-PMSG turbines. Converter failures are traditionally linked to the thermal loading of the power module. This paper

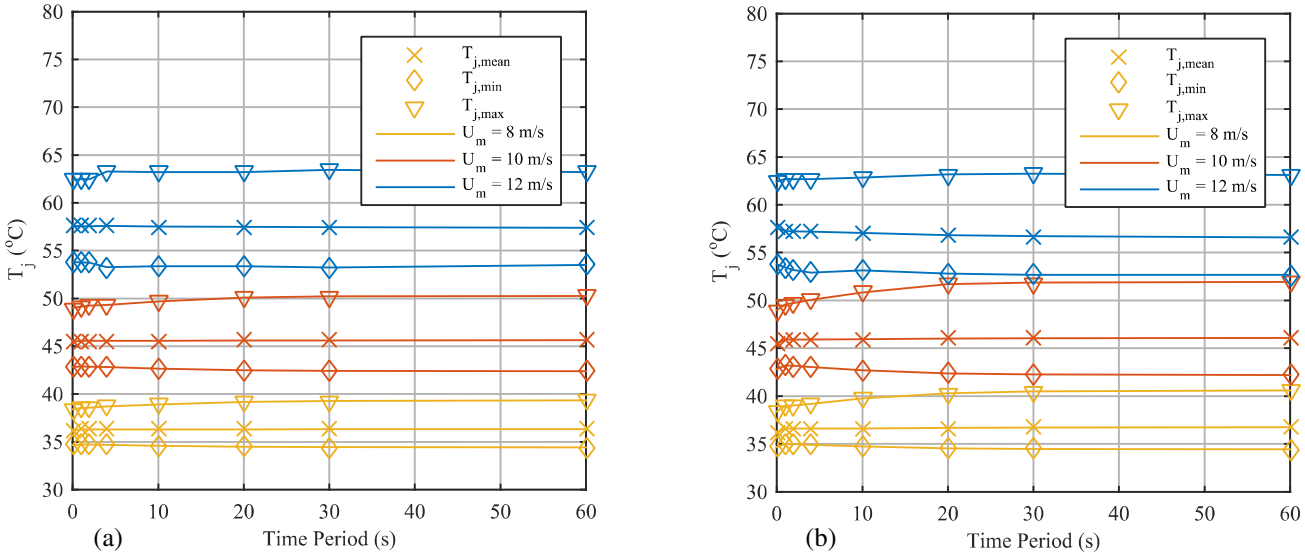

Figure 7: T_j response to square wave WSTS with varying time period, U_m and wave amplitude of (a) 1m/s, (b) 2m/s.

models the expected converter thermal loading when the turbine is subjected to various synthetic WSTS to explore the impact of wind conditions on power converter fatigue.

The thermal simulation has 3 main parts: a PMSG drive train model; a converter power loss model based on conduction and switching/RR; and a Cauer RC thermal equivalent circuit model. Both constant and square wave WSTS were tested and compared to manufacturing data and results in [11]. It was found that the model performed as expected compared to manufacturer's data. The diodes had greater thermal loading than the IGBTs, and this converter had higher mean T_j than in [11]. These preliminary results suggest that wind events of period >5s are critical to device thermal loading.

Future work will provide estimation of theoretical failure times and the most damaging wind speeds to the converter. The results will also be validated using an experimental rig.

References

[1] E. Davey and A. Nimmo. "Offshore Wind Cost Reduction, Pathways Study", (2012). Accessed [07/10/2015]. Available from: http://www.thecrownestate.co.uk/energy-and-infrastructure/offshore-wind-energy/working-with-us/strategic-workstreams/cost-reduction-study/.

[2] W. Musial and B. Ram. "Large-Scale Offshore Wind Power in the United States: Assessment of Opportunities and Barriers", (2010). Accessed [07/10/2015]. Available from: http://www.nrel.gov/docs/fy10osti/40745.pdf.

[3] J. Carroll, A. McDonald, and D. McMillan. "Failure rate, repair time and unscheduled O&M cost analysis of offshore wind turbines", *Wind Energy*. (2015).

[4] J. Carroll, A. McDonald, and D. McMillan. "Reliability Comparison of Wind Turbines With DFIG and PMG Drive Trains", *IEEE Transactions on Energy Conversion*. **30**(2), pp. 663. (2015).

[5] M. Spring, et al. "Top 30 Chart for wind turbine failure mechanisms", *EWEA Annual Event*, (2015).

[6] M. Bartram and R.W. De Doncker. "Doubly-fed-machines in wind-turbine systems: is this application limiting the lifetime of IGBT-frequency-converters?", *IEEE 35th Annual Power Electronics Specialists Conference*, (2004).

[7] K. Ma, et al. "Thermal loading and lifetime estimation for power device considering mission profiles in wind power converter", *IEEE Transactions on Power Electronics*. **30**(2), pp. 590-602. (2015).

[8] D. Zhou, et al. "Reliability and energy loss in full-scale wind power converter considering grid codes and wind classes", *IEEE Energy Conversion Congress and Exposition*, (2014).

[9] O.S. Senturk, et al. "Electro-thermal modeling for junction temperature cycling-based lifetime prediction of a press-pack IGBT 3L-NPC-VSC applied to large wind turbines", *IEEE Energy Conversion Congress and Exposition*, (2011).

[10] M. Musallam and C.M. Johnson. "Impact of different control schemes on the life consumption of power electronic modules for variable speed wind turbines", *14th European Conference on Power Electronics and Applications* (2011).

[11] E. Baygildina, et al. "Thermal loading of wind power converter considering dynamics of wind speed", *39th Annual Conference of the IEEE Industrial Electronics Society*, (2013).

[12] A. Isidoril, et al. "Thermal loading and reliability of 10-MW multilevel wind power converter at different wind roughness classes", *IEEE Transactions on Industry Applications*. **50**(1), pp. 484-494. (2014).

[13] F. Fuchs and A. Mertens. "Steady state lifetime estimation of the power semiconductors in the rotor side converter of a 2 MW DFIG wind turbine via power cycling capability analysis", *14th European Conference on Power Electronics and Applications*, (2011).

[14] E. Kostandyan and K. Ma. "Reliability estimation with uncertainties consideration for high power IGBTs in 2.3 MW wind turbine converter system", *Microelectronics reliability*. **52**(9), pp. 2403-2408. (2012).

[15] D. Weiss and H.-G. Eckel. "Fundamental frequency and mission profile wearout of IGBT in DFIG converters for windpower", *15th European Conference on Power Electronics and Applications*, (2013).

[16] C.J. Smith, et al. "Characterisation of Electrical Loading Experienced by a Wind Turbine Power Converter", *EWEA Annual Event* (2015).

[17] A. Hansen, et al. "Control of variable speed wind turbines with doubly-fed induction generators", *Wind Engineering*. **28**(4), pp. 411-432. (2004).

[18] SEMIKRON. "SKS B2 100 GD 69/11 - MA PB Datasheet", (2013). Accessed [07/12/2015]. Available from: http://www.semikron.com/dl/service-support/downloads/download/semikron-datasheet-sks-b2-100-gd-69-11-ma-pb-08800565.

[19] SEMIKRON. "SKiiP 2013 GB172-4DW V3 Datasheet", (2014). Accessed [08/12/2015]. Available from: http://www.semikron.com/dl/service-support/downloads/download/semikron-datasheet-skiip-2013-gb172-4dw-v3-20451248.

[20] P. Wyllie, *Electrothermal Modelling for Doubly Fed Induction Generator Converter Reliability in Wind Power*. Durham University Thesis. (2014).

[21] A. Wintrich, et al, *Application Manual Power Semiconductors*. 2011, Ilmenau, Germany: ISLE Verlag.

[22] SEMIKRON. "SKiiP 11NAB066V1 Datasheet", (2006). Accessed [18/12/2015]. Available from: http://www.semikron.com/dl/service-support/downloads/download/semikron-datasheet-skiip-11nab066v1-25230580.

[23] NXP. "AN11261: Using RC Thermal Models: Application note", (2014). Accessed [09/12/2015]. Available from: http://www.nxp.com/documents/application_note/AN11261.pdf.

[24] K.R. Shailesh. "Convert Foster Network to Cauer", (2014). Accessed [09/12/2015]. Available from: http://uk.mathworks.com/matlabcentral/fileexchange/46348-convert-foster-network-to-cauer/content//fostercauer.m.